PROCEEDINGS OF SCIENCE

Searches for monojets and monophotons with the ATLAS detector

Roger Caminal Armadans, on behalf of the ATLAS Collaboration*
Institut de Física d'Altes Energies (IFAE) - Edifici Cn,
Universitat Autònoma de Barcelona (UAB), E-08193 Bellaterra (Barcelona), Spain
E-mail: caminal@ifae.es

Searches for new phenomena in events with a high-energy jet or photon and missing transverse momentum in the final state are performed using events from proton-proton collisions at center of mass energies of 7 TeV and 8 TeV with the ATLAS experiment at the LHC. No excess of events beyond expectations from Standard Model processes is observed. New exclusion limits are obtained on the existence of large extra spatial dimensions, the pair production of dark matter candidates, and the associated production of light gravitinos and squark/gluinos in a gauge-mediated supersymmetry breaking model.

XXI International Workshop on Deep-Inelastic Scattering and Related Subject -DIS2013,
22-26 April 2013
Marseilles, France

*Speaker.

PoS(DIS 2013)119

1. Introduction

Events with an energetic jet of hadrons or an energetic photon and large missing transverse momentum in the final state constitute a clean and distinctive signature in searches for new physics at colliders. In particular, monojet and monophoton final states have been studied [1, 2, 3, 4, 5] in the context of searches for supersymmetry (SUSY), large extra spatial dimensions (LED), and dark matter (DM), to address some of the most fundamental questions in elementary particle physics and cosmology.

The Arkani-Hamed, Dimopoulos, and Dvali model (ADD) for LED [6] provides a possible solution to the mass hierachy problem. It explains the large difference between the electroweak scale $O(10^2$ GeV$)$ and the Plank scale, $M_{Pl} \sim O(10^{19}$ GeV$)$, by postulating the presence of n extra spatial dimensions of size R, and defining a fundamental Planck scale in $4+n$ dimensions, M_D, given by $M_{Pl} \sim M_D^{2+n} R^n$. An appropriate choice of R for a given n allows a value of M_D at the electroweak scale. The extra spatial dimensions are compactified, resulting in a Kaluza-Klein tower of massive graviton modes. At hadron colliders, the gravitons modes can be produced in association with an energetic photon or jet, but escape detection, leading to a monophoton or monojet final state.

The presence of a non-baryonic DM component in the Universe is inferred from the observation of its gravitational interactions [7], but its nature remains unknown. If weakly interacting massive particles (WIMPs) are produced in high energy proton-proton collisions, they do not interact with the detector and the event can be identified via the presence of an energetic photon or jet from initial-state radiation. The interaction of WIMPs with Standard Model (SM) particles is assumed to be driven by a very massive mediator and described using a non-renormalizable effective theory [8] with several operators. The vertex coupling is suppressed by an effective cut-off mass scale $M_* \sim M/\sqrt{g_1 g_2}$, where M denotes the mass of the mediator and g_1 and g_2 are the couplings of the mediator to the WIMP and the SM particles, respectively. Dark matter candidates are assumed to be Dirac fermions and different operators with scalar (D1, D11), vector (D5), axial-vector (D8), and tensor (D9) structure are considered. A WIMP χ with mass m_χ in the range between 1 GeV and a few TeV is a plausible candidate for DM.

In gauge mediated SUSY breaking (GMSB) scenarios [9, 10, 11], the gravitino $\tilde{G}$ (spin-$\frac{3}{2}$ superpartner of the graviton) is often considered the lighest supersymmetric particle (LSP) and a potential candidate for DM. Its mass is related to the SUSY breaking scale $\sqrt{F}$ and M_{Pl} via $m_{\tilde{G}} \propto F/M_{Pl}$. At hadron colliders, the cross sections for associated production of a gravitino and a squark ($pp \to \tilde{G}\tilde{q}+X$) or a gravitino and a gluino ($pp \to \tilde{G}\tilde{g}+X$) become relevant [12]. The cross sections depend on $m_{\tilde{G}}$ as $\sigma \sim 1/m_{\tilde{G}}^2$ and therefore provide the means to determine a lower bound on $m_{\tilde{G}}$. The decay of the gluino or squark into a gravitino and a gluon ($\tilde{g} \to \tilde{G}g$) or a gravitino and a quark ($\tilde{q} \to \tilde{G}q$), respectively, dominates [12], and the final state is characterized by the presence of a pair of gravitinos that escape detection and an energetic jet, leading to a monojet topology.

2. Searches in monojet final states

Searches in events with a very energetic jet and large missing transverse momentum, E_{T}^{miss}, are performed with 4.7 fb^{-1} of data recorded at $\sqrt{s} = 7$ TeV [13] and with 10.5 fb^{-1} of $\sqrt{s} = 8$ TeV

data recorded in 2012 [14]. The events are collected using an inclusive E_{T}^{miss} trigger and further required to have a reconstructed primary vertex with at least two associated tracks. Requirements on the fraction of the transverse momentum, p_{T}, of the jet carried by charged tracks, the fraction of the jet energy contained in the electromagnetic layers of the calorimeter and the η range[1] suppress jets produced by cosmic rays or beam-background muons. No more than two jets with $p_{\mathrm{T}} >$ 30 GeV and $|\eta| < 4.5$ are allowed and the leading jet has to be within $|\eta| < 2$. In order to suppress multijet events, the $E_{\mathrm{T}}^{miss}$and the p_{T} of the second leading jet are required to be well separated, $\Delta\phi(E_{\mathrm{T}}^{miss}, p_{\mathrm{T\,sub\text{-}leading}}) > 0.5$. Furthermore, in order to reject events coming from the production of W or Z bosons in association with jets, the events are required to have no electrons or muons in the final state. Four overlapping signal regions are defined by symmetric lower cuts in $E_{\mathrm{T}}^{miss}$and p_{T} of the leading jets, with values of 120 GeV, 220 GeV, 350 GeV and 500 GeV, called SR1-SR4, respectively.

The Standard Model background contributions are dominated by the production of Z bosons together with jets where the boson decays to two neutrinos, $Z(\nu\nu)+$jets. Other significantly contributing processes are $W(l\nu)+$jets $(l = e,\mu,\tau)$ with the decay leptons escaping detection or, in case of $W(\tau\nu)+$jets, the τ decaying hadronically. $Z/\gamma^*(l^+l^-)+$jets $(l = e,\mu,\tau)$ contributes when neither lepton is identified or both are outside the detector acceptance. These contributions make up about 97% of the total background and are normalized using scale factors determined in control samples in data, with identified electrons or muons in the final state and with the same requirements in p_{T}, subleading jet vetoes, and E_{T}^{miss}. Top quark and diboson production are taken directly from the simulation and the multijet contribution is estimated using fully data-driven techniques. The dominant systematic uncertainties associated with the electroweak background estimates come from the absolute jet and E_{T}^{miss} energy scales, as well as theoretical uncertainties on the shape of W plus jets kinematic distributions and the ratio of Z and W plus jets production cross sections. The total systematic uncertainty in the different signal regions is 3.4% in SR1, 4.4% in SR2, 6.8% in SR3 and 11.1% in SR4.

Figure 1 shows the E_{T}^{miss} distribution in SR1. Good agreement is observed between the data and the SM predictions. The results are translated into limits[2] on the parameters of the ADD LED model. Figure 2 shows the 95% confidence level (CL) lower limit on M_D versus n, taking into account theoretical and experimental uncertainties. M_D values below 4.17 TeV for $n = 2$ and 2.51 TeV for $n = 6$ are excluded at 95% CL.

The same results can be translated into limits in the suppression scale M_* for WIMP pair production for all operators, probed as a function of the WIMP mass m_χ. In the case of the scalar D1 spin-independent operator, values for M_* below 30 GeV and 6 GeV are excluded at 90% CL for m_χ equal to 1 GeV and 1.3 TeV respectively. For the vector D5 (scalar D11) spin-independent operators, values for M_* below 687 GeV and 173 GeV (347 GeV and 118 GeV) are excluded at 90% CL for m_χ equal to 1 GeV and 1.3 TeV respectively. Values for M_* below 687 GeV and 110 GeV (1353 GeV and 240 GeV) are excluded at 90% CL for the axial-vector D8 (tensor D9)

[1] ATLAS uses a right-handed coordinate system with its origin at the nominal interaction point (IP) in the centre of the detector and the z-axis along the beam pipe. The x-axis points from the IP to the centre of the LHC ring, and the y-axis points upward. Polar coordinates (r,ϕ) are used in the transverse (x,y)-plane, ϕ being the azimuthal angle around the beam pipe. The pseudorapidity is defined in terms of the polar angle θ as $\eta = -\ln\tan(\theta/2)$.

[2] Limits are computed using the CL_s method [15].

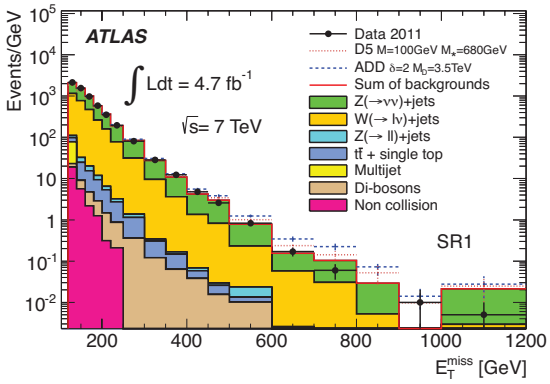

Figure 1: E_{T}^{miss} distribution for signal region SR1 [13]. Signal distributions for ADD and WIMP samples for cross sections at the excluded limit are drawn as dashed lines on top of the predicted background distributions.

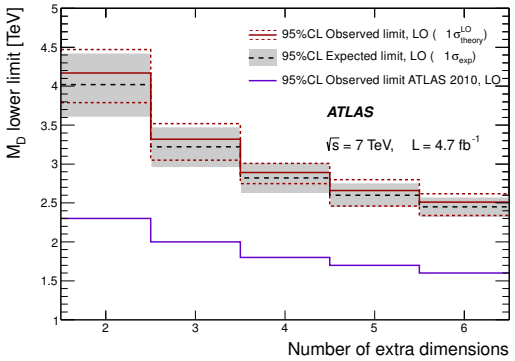

Figure 2: 95% CL lower limits on M_D for different numbers of extra dimensions based on SR4 [5]. Observed and expected limits including all but the theoretical signal uncertainties are shown as solid and dashed lines, respectively. The grey $\pm 1\sigma$ band around the expected limit is the variation expected from statistical and experimental systematic uncertainties on SM and signal processes. The impact of the theoretical uncertainties is shown by the red small-dashed $\pm 1\sigma$ limits. The previous ATLAS limit is also shown for comparison.

operator.

In the effective operator approach, the ATLAS bounds on M_* for a given m_χ can be converted to bounds on WIMP-nucleon scattering cross sections, which are probed by direct dark matter detection experiments. These bounds describe scattering of WIMPs from nucleons at a very low momentum transfer, of the order of a keV. Figure 3 shows the 90% CL upper limits on the nucleon-WIMP cross sections as a function of m_χ for spin dependent (left) and spin independent (right) models. D8 and D9 (spin-dependent) cross section limits are significantly better than those from direct-detection experiments. The spin-independent ATLAS limits are particularly relevant in the low m_χ region (< 10 GeV) where direct search experiments suffer from kinematic suppression. Should DM particles couple exclusively to gluons via D11, then the collider limits would be competitive up to m_χ of about 20 GeV, and remain important over almost the full m_χ range covered.

The monojet analysis has been updated with 10.5 fb^{-1} of 8 TeV data [14]. The analysis strategy and the event selection criteria follow closely that of the 7 TeV analysis [13]. Good agreement is observed again between data and SM predictions. This analysis improves the limits on the parameters of ADD LED model, the suppression scale on WIMP pair production and WIMP-nucleon scattering cross sections determined with the 7 TeV analysis. The results are also translated into limits on the cross section for the associated production of gravitinos with squarks or gluinos in the final state. Figure 4 shows the 95% CL limit on the gravitino mass as a function of the squark mass for degenerate squark/gluino masses. 95% CL lower bounds on the gravitino mass in the range between 3×10^{-4} eV and 3×10^{-5} eV are set on the squark and gluino masses. The limits on the gravitino mass can be translated into a limit on the SUSY breaking scale $\sqrt{F}$ ($m_{\tilde{G}} \propto F/M_{Pl}$).

Values of $\sqrt{F}$ below 640 GeV are excluded at 95% CL, extending very significantly previous LEP and Tevatron results [16].

3. Searches in monophoton final states

Searches for new physics in events with an energetic photon and large missing transverse momentum are a priori less sensitive compared to similar searches in the monojet channel, but they allow access to a completely different final state and an independent cross check of monojet results. This search is performed with 4.6 fb^{-1} of data recorded at 7 TeV [17], collected using an inclusive E_{T}^{miss} trigger. Offline the events are required to have $E_{\mathrm{T}}^{miss} > 150$ GeV and a photon with transverse momentum $p_{\mathrm{T}} > 150$ GeV and $|\eta| < 2.37$. The photon candidate must pass tight identification criteria based on shower shapes measured in the electromagnetic calorimeter and on the energy leakage into the hadron calorimeter, and is required to be isolated. Jets are defined using the anti-k_t jet algorithm with the distance parameter set to $R = 0.4$. Events with more than one jet with $p_{\mathrm{T}} > 30$ GeV and $|\eta| < 4.5$ are rejected. The reconstructed photon, E_{T}^{miss} and jets (if any) are required to be well separated in the transverse plane with $\Delta\phi(\gamma, E_{\mathrm{T}}^{miss}) > 0.4$, $\Delta R(\gamma, \mathrm{jet}) > 0.4$, and $\Delta\phi(\mathrm{jet}, E_{\mathrm{T}}^{miss}) > 0.4$. Additional quality criteria are applied to ensure that jets and photons were not produced by noisy calorimeter cells. Electron (muon) candidates are required to have $p_{\mathrm{T}} > 20$ GeV and $|\eta| < 2.47$ ($p_{\mathrm{T}} > 10$ GeV and $|\eta| < 2.4$), and to pass the medium (combined) criteria [18]. Events with identified electrons or muons are vetoed to reject mainly $W/Z+$jets and $W/Z+\gamma$ background processes with charged leptons in the final state.

The normalization of the MC predictions for the dominant $W/Z+\gamma$ background processes are determined in a similar way as for the monojet analysis. A $\gamma+\mu+E_{\mathrm{T}}^{miss}$ control sample with an identified muon in the final state is defined by inverting the muon veto in the nominal event selection criteria. The scale factor is defined as the ratio between the data and the given MC prediction, after the contributions from the other background processes are subtracted. Also dedicated studies are performed to determine, using data, the probability for electrons or jets to be identified as photons in the final state, which result in data-driven estimates of $W/Z+$jets background contributions. The $\gamma+$jet and multi-jet background contributions are determined from data using a control sample with the nominal selection criteria and at least one jet with $p_{\mathrm{T}} > 30$ GeV and $\Delta\phi(\mathrm{jet}, E_{\mathrm{T}}^{miss}) < 0.4$.

The dominant sources of systematic uncertainties in the electroweak backgrounds are the uncertainty on the abolute jet energy scale and resolution for low p_{T} jets and unclustered energy in the calorimeter, the dependence of the predicted $W/Z+\gamma$ backgrounds on the parton shower and hadronization model used in the MC simulations and the subtraction of pileup contributions. The different sources of uncertainty are added in quadrature, resulting in a total 15% uncertainty on the background prediction.

The data are in agreement with the SM prediction. Figure 5 shows the measured E_{T}^{miss} distribution compared to the background predictions. The figure indicates the impacts of ADD LED and WIMP scenarios. These results are translated into 95% CL limits on the parameters of the ADD LED model. Figure 6 shows the expected and observed 95% CL upper limits on M_D as a function of n. Values of M_D below 1.74 TeV ($n = 2$ or 3), 1.78 TeV ($n = 4$), 1.82 TeV ($n = 5$), and 1.87 TeV ($n = 6$) are excluded at 95% CL.

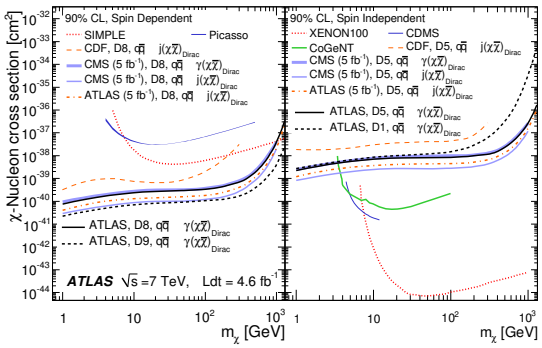

Figure 3: Monojet and monophoton 90% CL upper limits on the nucleon-WIMP cross section as a function of m_χ for spin-dependent (left) and spin-independent (right) interactions [17]. The results are compared with previous monojet and monophoton results at colliders and results from direct detection experiments.

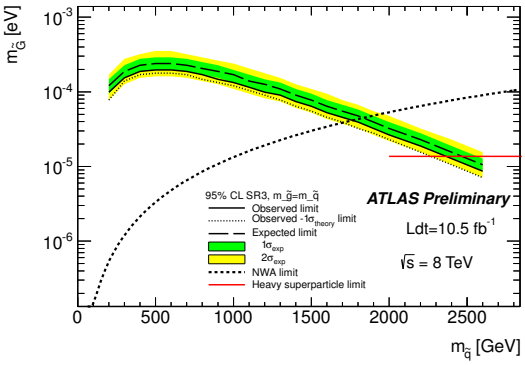

Figure 4: Observed (solid line) and expected (dashed line) 95% CL lower limits on the gravitino mass as a function of the squark or gluino masses for degenerate squark/gluino masses [14]. The dashed-dotted line defines the validity of the narrow-width approximation. The shaded bands around the expected limit indicate the expected $\pm 1\sigma$ and $\pm 2\sigma$ ranges of limits in the absence of a signal. The solid red line denotes the current limit from LEP on the gravitino mass assuming very heavy squarks/gluino.

Limits on the scale M_* are also extracted. In the case of the vector D5 spin-independent operator, values for M_* below 585 GeV and 156 GeV are excluded at 90% CL for m_χ equal to 1 GeV and 1.3 TeV respectively. Values for M_* below 585 GeV and 100 GeV (794 GeV and 188 GeV) are excluded for the axial-vector D8 (tensor D9) spin-dependent operator for m_χ equal to 1 GeV and 1.3 TeV respectively. Figure 3 shows 90% CL upper limits on the nucleon-WIMP cross section as a function of m_χ. In the case of spin-independent interaction, nucleon-WIMP cross sections above 2.2×10^{-39} cm^2 and 1.7×10^{-36} cm^2 are excluded at 90% CL for $m_\chi = 1$ GeV and $m_\chi = 1.3$ TeV respectively. Spin-dependent interactions cross sections in the range 7.6×10^{-41} cm^2 to 3.4×10^{-37} cm^2 (2.2×10^{-41} cm^2 to 2.7×10^{-38} cm^2) are excluded at 90% CL for the D8 (D9) operator and m_χ varying between 1 GeV and 1.3 TeV.

4. Conclusion

This contribution presents the results of searches for new phenomena in events with a jet or a photon and missing transverse momentum in the final state, obtained from proton-proton collision data at center of mass energies of 7 TeV and 8 TeV. Data-driven techniques have been used to determine the most important Standard Model backgrounds for each analysis. Good agreement is observed between data and the SM predictions in all cases. The results are translated into improved limits on different scenarios for new physics, including large extra spatial dimensions, WIMP pair production, and the production of gravitinos in a gauge mediated SUSY breaking model.

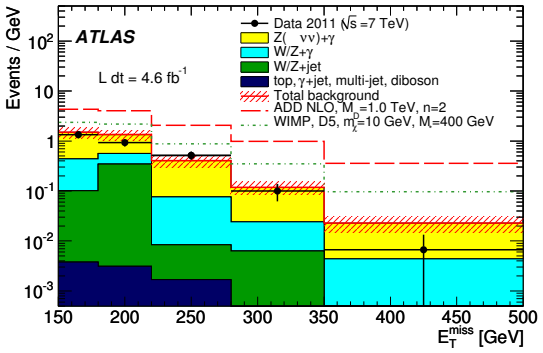

Figure 5: The measured ETmiss distribution (black dots) compared to the SM (solid lines), SM+ADD LED (dashed lines), and SM+WIMP (dotted lines) predictions, for two particular ADD LED and WIMP scenarios [17]. The band around the total background prediction includes uncertainties on the data-driven background estimates and statistical uncertainties on the MC samples.

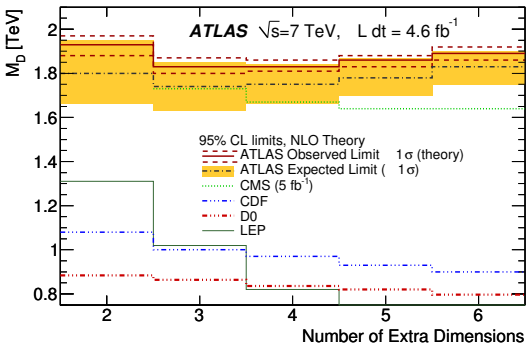

Figure 6: Observed (solid lines) and expected (dashed-dotted lines) 95% CL limits on M_D as a function of the number of extra spatial dimensions n in the ADD LED model [17]. The dashed lines around the observed limit indicate the impact of the $\pm 1\sigma$ NLO theoretical uncertainty on the limit computation. The shaded band indicates the expected $\pm 1\sigma$ range of limits in the absence of a signal. The results are compared with previous results (other lines).

References

[1] D0 Collaboration, V. Abazov et al., Phys.Rev.Lett. **101** (2008) 011601, arXiv:0803.2137 [hep-ex].

[2] CDF Collaboration, T. Aaltonen et al., Phys.Rev.Lett. **101** (2008) 181602, arXiv:0807.3132 [hep-ex].

[3] CDF Collaboration, T. Aaltonen et al., Phys.Rev.Lett. **108** (2012) 211804, arXiv:1203.0742 [hep-ex].

[4] CMS Collaboration, Phys.Rev.Lett. **108** (2012) 261803, arXiv:1204.0821 [hep-ex].

[5] ATLAS Collaboration, Phys.Lett. **B705** (2011) 294–312, arXiv:1106.5327 [hep-ex].

[6] N. Arkani-Hamed, S. Dimopoulos, and G. Dvali, Phys.Lett. **B429** (1998) 263–272, arXiv:hep-ph/9803315 [hep-ph].

[7] WMAP Collaboration, E. Komatsu et al., Astrophys.J.Suppl. **192** (2011) 18, arXiv:1001.4538 [astro-ph.CO].

[8] J. Goodman, M. Ibe, A. Rajaraman, W. Shepherd, T. M. Tait, et al., Phys.Rev. **D82** (2010) 116010, arXiv:1008.1783 [hep-ph].

[9] G. Giudice and R. Rattazzi, Phys.Rept. **322** (1999) 419–499, arXiv:hep-ph/9801271 [hep-ph].

[10] R. Casalbuoni, S. De Curtis, D. Dominici, F. Feruglio, and R. Gatto, Phys.Lett. **B215** (1988) 313.

[11] P. Fayet, Phys.Lett. **B70** (1977) 461.

[12] M. Klasen and G. Pignol, Phys.Rev. **D75** (2007) 115003, arXiv:hep-ph/0610160 [hep-ph].

[13] ATLAS Collaboration, JHEP **1304** (2013) 075, arXiv:1210.4491 [hep-ex].

[14] ATLAS Collaboration, ATLAS-CONF-2012-147, http://cds.cern.ch/record/1493486/ .

[15] A. L. Read, J.Phys. **G28** (2002) 2693–2704.

[16] CDF Collaboration, T. Affolder et al., Phys.Rev.Lett. **85** (2000) 1378–1383, arXiv:hep-ex/0003026 [hep-ex].

[17] ATLAS Collaboration, Phys.Rev.Lett. **110** (2013) 011802, arXiv:1209.4625 [hep-ex].

[18] ATLAS Collaboration, Phys.Rev. **D85** (2012) 072004, arXiv:1109.5141 [hep-ex].